Supplemental Online Material

Chemical forms of uranium evaluated by thermodynamic calculation associated with distribution of core materials in the damaged reactor pressure vessel

Hirotomo Ikeuchi[a*], Kimihiko Yano[a], Tadahiro Washiya[a].

[a] Collaborative Laboratories for Advanced Decommissioning Science, Japan Atomic Energy Agency, 4-33, Muramatsu, Tokai-mura, Naka-gun, Ibaraki 319-1194, Japan

[*]Corresponding author. Email: ikeuchi.hirotomo@jaea.go.jp

Appendix A. Comparison between Thermodynamic Calculation and Experimental Data

The main objective is to gain an insight on to which extent the thermodynamic calculation could reproduce the experimentally observed solid phases. Given the information on the average elemental composition of the solidified melt and the constituent phases in it, 8 experimental campaigns were selected as the comparison cases. The calculation conditions (elemental compositions and temperatures) are shown in Case A01 to A08 of Table A1. For each case, the temperature step calculation was performed being based on the lever rule. The fraction of solid phases calculated at the solidus temperature, T_{sol}, are summarized in Table A2, being compared with the experimental data.

Construction of the calculation conditions and results for each case are detailed in the following sections.

A.1. U–Zr–O ternary system for the UO_2–Zr interaction

The experimental study by Quaini et al.[9] were selected as the cases for solidification of the U–Zr–O melt (cases A01 to A05 in Table A1). The initial batch consisted of metallic U, ZrO_2, and Zr were melted in the tungsten resistance furnace under the inert atmosphere at approximately 2567 K. In the specific range of compositions, the melt was separated into two immiscible liquids: O-rich melt and O-poor melt. It is highly expected that those two liquids had been solidified separately during the rapid cooling because the boundaries between the two phases were clearly visible even after the complete solidification. Therefore, solidification calculations were performed individually for the O-rich melt and the O-poor melt (as indicated in the cases A02 to A05 in Table A1). Average compositions of U, Zr, and O in the solidified melt measured by the electron probe microanalysis (EPMA) were used for the present calculation. Thermodynamic calculations were performed using the U–Zr–O ternary system of the NUCLEA database.

Three types of solid phases were identified in the results of calculation: *F*-$(U,Zr)O_{2-x}$,

α-(Zr,U)(O), and bcc-(U,Zr) alloy, showing qualitative agreement with experimental data (A01 to A05 of Table A2). For the cases A01, A02, and A04, phase fractions of the α-(Zr,U)(O) calculated (72.1, 54.7, and 41.5 mol%, respectively) were reasonably agreed with the experimental values (76, 54, and 41 mol%, respectively). The atomic ratio of U/(U+Zr) in the α-(Zr,U)(O) calculated for the cases A01 to A05 was in the range of 0.02 to 0.03, which is similar to experimental values (0.02 to 0.04). Fraction of U in the α-(Zr,U)(O) seems to be well reproduced by the calculation.

A.2. U–Zr–O–Fe quaternary system for the UO_2–Zr–ZrO_2–SS interactions

The "MA-1" test, performed in the framework of Material Scaling project of Organisation for Economic Co-operation and Development (OECD/MASCA) [11,12], was selected as a typical case for the UO_2, Zr, ZrO_2, and SS interactions (case A06 in Table A1). The mixture of UO_2, Zr, and ZrO_2 was initially heated and kept at approximately 2773 K in the cold crucible induction furnace under the inert atmosphere after which the SS was added stepwise. This experiment indicated the liquid immiscibility as similar to the cases A02 to A05. Since the O-rich melt resembles the U–Zr–O ternary system discussed in the previous section, we especially focus on the O-poor melt. Average compositions of U, Zr, O, and Fe (including Cr and Ni from SS) in the O-poor melt measured by the X-ray fluorescence spectrometry (XRF, for the metallic elements), and the spark source mass spectrometry (SS-MS, for O) were used for the calculation. Thermodynamic calculations on the UO_2, Zr, ZrO_2, and SS interactions were performed using the U–Zr–O–Fe quaternary system of the NUCLEA database.

Four types of solid phases were identified in the result of calculation: two Fe_2Zr-type Laves phases with Zr-rich and U-rich compositions, *F*-$UO_{2.0}$, and γ-Fe, showing qualitative agreement with experimental data (A06 of Table A2). Though phase fractions were not reported, the calculated atomic ratios of U/(U+Zr) for the U-rich and Zr-rich Laves phase

(0.74 and 0.11, respectively) were similar to experimental values (0.72 and 0.14, respectively), Therefore the partitioning of U among the two phases could be well reproduced.

A.3. U–Zr–O–Fe quaternary system for the UO_2–ZrO_2–FeO_x interactions

Two experiments were selected for the U–Zr–O–Fe system with oxidizing conditions in which the UO_2–ZrO_2–FeO_x interactions prevail.

First one comes from the data reported by Almjashiv et al.[22] in which the eutectic point and eutectic compositions of the UO_2–ZrO_2–FeO_{1+x} melt were investigated by melting the mixture of UO_2, ZrO_2, FeO_{1+x}, and metallic Fe in the cold crucible induction furnace under inert atmosphere. The average elemental composition in the eutectic area measured with the energy-dispersive X-ray spectroscopy (EDX) were used for the input condition (case A07 in Table A1). The solid phases calculated at the T_{sol} consist of three major oxides ($FeO_{1.05}$-wüstite, *F*-(U,Zr,Fe)O_2, and *T*-(Zr,U,Fe)O_2) and small fraction of metallic Fe, showing qualitative agreement with experimental data (A07 in Table A2). The ZrO_2 contents and FeO contents in the UO_2-rich fluorite phase (0.10 and 0.18, respectively) is consistent with the experimental ones (0.11 and 0.10, respectively). The authors [22] argued that the UO_2 and FeO contents in the ZrO_2-rich tetragonal phase determined by EDX could be overestimated owing to the contribution from surrounding phases. Considering the probable error in the measurement of ZrO_2-rich phase, partitioning of U among the UO_2-rich, ZrO_2-rich and FeO-rich oxides could be roughly evaluated.

The second one is associated with highly oxidizing conditions. As reported by Petrov et al. [23] (Case S08 in Table S1), the mixture of UO_2, ZrO_2, Fe_2O_3, and small addition of Cr_2O_3 (~3.3 wt.%) were melted and solidified in the cold crucible inductive furnace under air atmosphere. In this case, considerable gradient of oxygen activity could have been existed in the melt[23]. To consider the effect of the variable oxygen activity in the melt on the calculation of solid phases, thermodynamic calculations on UO_2–ZrO_2–Fe_2O_3 interactions, in

which the Cr_2O_3 was included in Fe_2O_3 for simplicity, were performed by considering two different scenarios on the oxygen amount in the melt. The first scenario, designated as case A08(1) in Table A1, assumes the constant amount of oxygen fixed at the initial batch composition (UO_2 + ZrO_2 + Fe_2O_3). This assumption could provide the lower limit of the oxygen amount in the melt. The second scenario, which is close to the upper limit of oxygen amount in the melt, assumes the oxidic melt equilibrated with air (case S08(2) in Table S1). To implement this assumption, step calculation was performed separately at the high temperature region and the low temperature region in the following way. At the temperatures higher than the T_{sol}, constant $p(O_2)$ of 0.21 atm was assumed (equivalent to that in air) to determine the amount of O in the melt equilibrated with air. Once the amount of O was determined at the T_{sol}, the amount of O was fixed at that value, and normal step calculation was performed at the temperatures lower than the T_{sol}.

Property diagrams calculated using the two composition types (A08(1) and A08(2)) are shown in Figure A1. According to the XRD analysis shown in Table A2, six solid phases were identified in the ingot: U_3O_8, $UO_{2.2}$, *T*-ZrO_2, Fe_2O_3, Fe_3O_4, and $FeUO_4$, and each phase can be found in the calculated property diagrams. However, the coexistence of six phases indicates that the solidification at highly oxidizing condition cannot be described by single thermodynamic conditions. Indeed, the calculated property diagrams indicate that the $FeUO_4$ appears only at low temperature domain when assuming the high oxygen amount in the melt (see Figure A1(b)). This case illustrates that thermodynamic calculation should be iterated considering widely variable conditions such as the oxygen potential and temperatures.

Table A1 Calculation conditions for the previous solidification experiments

Case No.	Elemental composition [mol%]				Range of temperature	ref. info.
	U	Zr	O	Fe		
U-Zr-O						
A01	10.2	50.7	39.1		up to 2567K	OUZr_1 in [9]
A02	13.9	40.1	46.0		up to 2567K	OUZr_2 (O-rich melt) in [9]
A03	16.2	53.6	30.2		up to 2567K	OUZr_2 (O-poor melt) in [9]
A04	17.3	32.0	50.7		up to 2567K	OUZr_3 (O-rich melt) in [9]
A05	28.0	48.4	23.6		up to 2567K	OUZr_3 (O-poor melt) in [9]
U-Zr-Fe-O (sub-oxidized)						
A06	15.83	10.04	1.64	72.50	up to 3000 K[a]	MA-1 (O-poor melt) in [11,12]
U-Zr-Fe-O (fully oxidizied)						
A07	1.83	2.11	51.97	44.09	up to 2400 K[a]	Eutectics in UO_2–ZrO_2–FeO_{1+x} in [22]
A08 (1)	8.56	7.86	63.28	20.29	up to 3000 K[a]	K-4 composition in [23]
(2)	8.56	7.86	$p(O_2)$ = 0.21atm	20.29	T > Tsol (= 1674 K)	K-4 composition in [23]
	8.37	7.68	64.11	19.84	T < Tsol (= 1674 K)	

Table A2 Comparison between the calculation and the experimental data

Case	Calc. Fraction Formula	Exp. Fraction Formula
A01	T_{liq} = 2268 K, Primary phase: *F*-$(U_{0.31}Zr_{0.69})O_{1.7}$ T_{sol} = 1702 K 27.8 mol% *F*-$(U_{0.98}Zr_{0.02})O_{2.0}$ 72.1 *α*-$(Zr_{0.98}U_{0.02})O_{0.40}$ 0.1 *bcc*-$(U_{0.51}Zr_{0.49})$	T_{max} = 2567 K 23 mol% $(U_{0.86}Zr_{0.14})O_{1.8}$ 76 *α*-$(Zr_{0.97}U_{0.03})O_{0.34}$ 1 $(U_{0.96}Zr_{0.04})$-alloy
A02	T_{liq} = 2389 K, Primary phase: *F*-$(U_{0.53}Zr_{0.47})O_{1.7}$ T_{sol} = 2024 K 45.3 mol% *F*-$(U_{0.81}Zr_{0.19})O_{1.9}$ 54.7 *α*-$(Zr_{0.97}U_{0.03})O_{0.43}$	T_{max} = 2567 K 46 mol% $(U_{0.77}Zr_{0.23})O_{1.8}$ 54 *α*-$(Zr_{0.96}U_{0.04})O_{0.35}$
A03	T_{liq} = 2274 K, Primary phase: *F*-$(U_{0.54}Zr_{0.46})O_{1.7}$ T_{sol} = 1702 K 18.1 mol% *F*-$(U_{0.98}Zr_{0.02})O_{2.0}$ 63.5 *α*-$(Zr_{0.98}U_{0.02})O_{0.40}$ 18.4 *bcc*-$(U_{0.51}Zr_{0.49})$	T_{max} = 2567 K ND $(U_{0.92}Zr_{0.08})O_{2.0}$ ND *α*-$(Zr_{0.97}U_{0.03})O_{0.37}$ ND $(U_{0.91}Zr_{0.09})$-alloy
A04	T_{liq} = 2463 K, Primary phase: *F*-$(U_{0.61}Zr_{0.39})O_{1.7}$ T_{sol} = 2025 K 58.5 mol% *F*-$(U_{0.81}Zr_{0.19})O_{1.9}$ 41.5 *α*-$(Zr_{0.97}U_{0.03})O_{0.43}$	T_{max} = 2567 K 59 mol% $(U_{0.87}Zr_{0.13})O_{1.9}$ 41 *α*-$(Zr_{0.96}U_{0.04})O_{0.35}$
A05	T_{liq} = 2431 K, Primary phase: *F*-$(U_{0.58}Zr_{0.42})O_{1.7}$ T_{sol} = 1702 K 18.5 mol% *F*-$(U_{0.98}Zr_{0.02})O_{2.0}$ 39.5 *α*-$(Zr_{0.98}U_{0.02})O_{0.40}$ 42.0 *bcc*-$(U_{0.51}Zr_{0.49})$	T_{max} = 2567 K ND $(U_{0.9}Zr_{0.1})O_2$ ND *α*-$(Zr_{0.97}U_{0.03})O_{0.37}$ ND $(U_{0.94}Zr_{0.06})$
A06	T_{liq} = 2846 K, Primary phase: *F*-$(U_{0.67}Zr_{0.33})O_{1.9}$ T_{sol} = 1342 K 15.6 wt% $Fe_{2.3}(U_{0.11}Zr_{0.89})$-Laves 68.6 $Fe_{2.0}(U_{0.75}Zr_{0.25})$-Laves 13.3 *γ*-Fe 2.5 *F*-$UO_{2.0}$	T_{max} = 2773 K ND $(Fe_{0.76}Cr_{0.14}Ni_{0.1})_{2.4}(U_{0.14}Zr_{0.86})$ ND $(Fe_{0.76}Cr_{0.1}Ni_{0.14})_{2.2}(U_{0.72}Zr_{0.28})$ ND $(Fe_{0.55}Cr_{0.43}Ni_{0.02})$ alloy ND $(U_{0.87}Zr_{0.13})O_2$
A07	T_{liq} = 1801 K, Primary phase: *δ*-Fe T_{sol} = 1564 K 76.9 wt% $FeO_{1.05}$-wüstite 13.5 *F*-$(U_{0.72}Zr_{0.1}Fe_{0.18})O_{1.8}$	 T_{eut} = 1583K ND $FeO_{1.059}$-wüstite ND $(U_{0.79}Zr_{0.11}Fe_{0.1})O_2$

	6.6 T-$(U_{0.05}Zr_{0.93}Fe_{0.02})O_{2.0}$ 3.0 γ-Fe	ND $(U_{0.21}Zr_{0.58}Fe_{0.21})O_2$[a]
A08	Only results of the case A08(2) are mentioned here. T_{liq} = 2050 K, Primary phase: T-$(U_{0.06}Zr_{0.92}Fe_{0.02})O_{2.0}$ T_{sol} = 1674 K 48.0 wt% U_3O_8 20.9 T-$(U_{0.01}Zr_{0.94}Fe_{0.05})O_{2.0}$ 31.1 $FeO_{1.33}$-spinel T_{trans} = 1321 K ($U_4O_9 + U_3O_8 + FeO_{1.5} \rightarrow FeUO_4$) 19.6 wt% M-ZrO_2 43.9 U_4O_9 4.7 $FeUO_4$ 31.8 $FeO_{1.5}$-hematite T_{trans} = 560 K ($U_4O_9 + 2FeO_{1.5} \rightarrow 2FeUO_4 + 2UO_2$) 21.7 wt% F-$UO_{2.0}$ 19.6 M-ZrO_2 33.3 $FeUO_4$ 25.4 $FeO_{1.5}$-hematite	(Determined from XRD analysis) 4 wt% U_3O_8 23 $UO_{2.2}$ 27 T-ZrO_2 20 Fe_3O_4 15 Fe_2O_3 10 $FeUO_4$

ND, Not determined.

a, The U and Fe contents are expected to have been overestimated due to the contribution from surrounding phases.

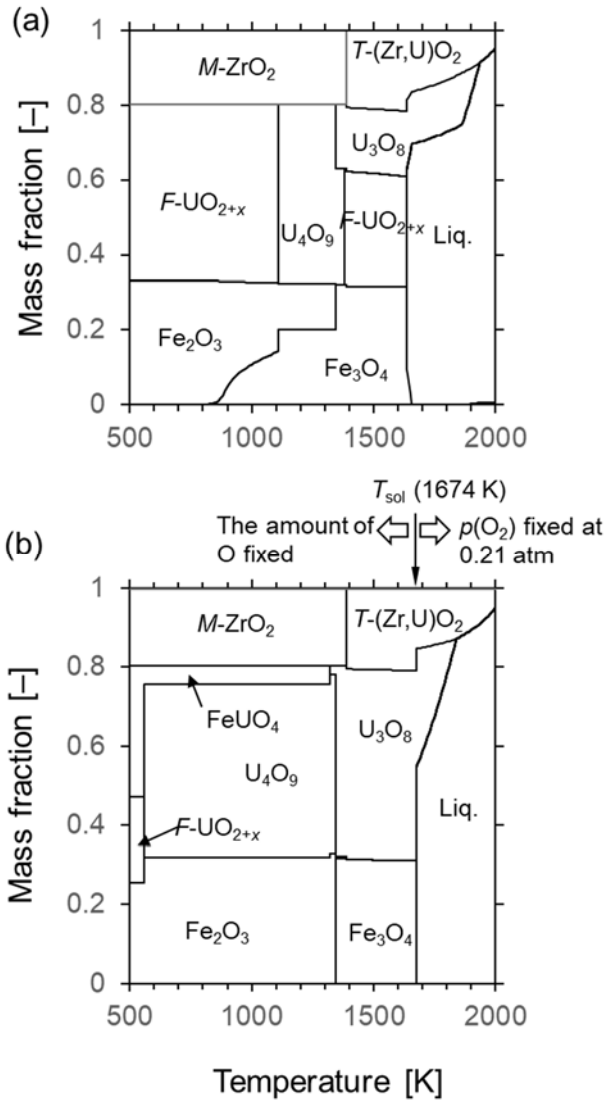

Figure A1 Calculated property diagrams for the UO_2–ZrO_2–Fe_2O_3 in air: (a), Case A08(1); and (b), Case A08(2).

Appendix B. Schematic Diagrams of Core Degradation Behavior Calculated with the Severe Accident Analyses

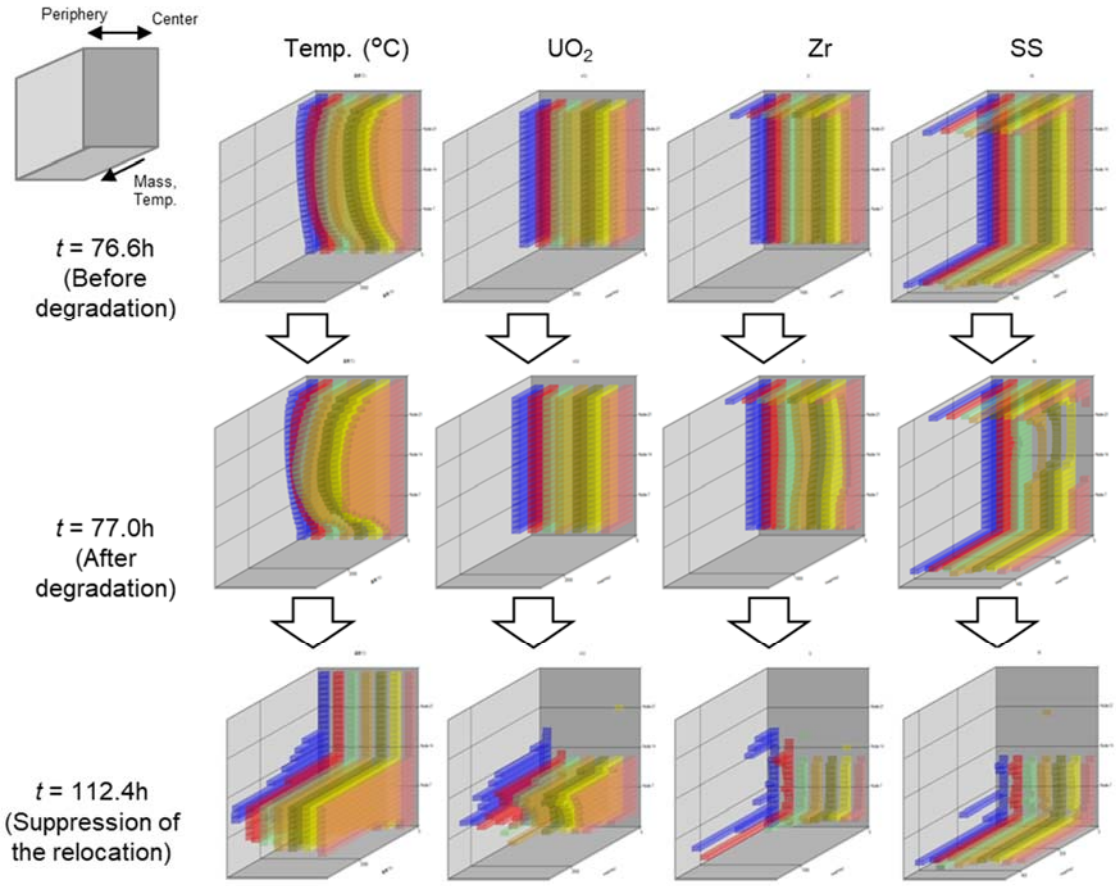

Brief description of the core degradation

- The core began degrading at approximately 77 hours after reactor shutdown, transferring significant amounts of SS mass through eutectic reaction with B_4C. Some part of the Zircaloy claddings was oxidized by steam though the oxidized mass is not shown here.
- The UO_2 and Zr located in the upper half of the active fuel region then collapsed and accumulated on the core support plate.
- The temperature rose to approximately 3100 K, sufficient for molten pool formation.
- After 112.4 h, the relocation of the core materials became less dramatic than in the earlier stages.

Figure B1. Relocation of core materials during the accident at 1F-2 in Case 1, calculated by MAAP5 code.

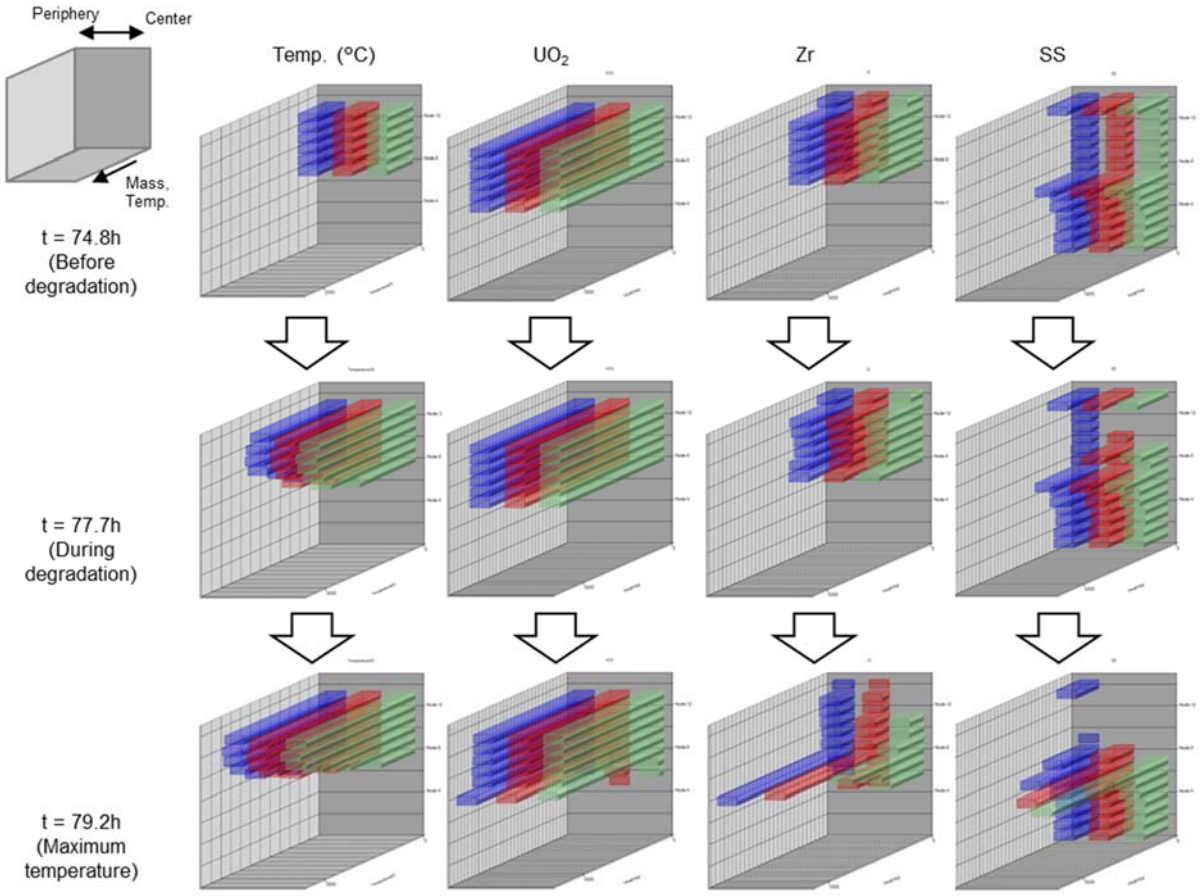

Brief description of the core degradation

- Similarly to Case 1, Zry oxidation and the preferential relocation of SS occurred in the early stage of core degradation (t = 77.7 h in the figure).
- The maximum temperature throughout the core increased up to 2400 K, causing relocation of UO_2 and Zry (t = 79.2 h in the figure).
- At the launch of water injection, the temperature began decreasing monotonically, suppressing the relocation.

Figure B2. Relocation of core materials during the accident at 1F-2 in Case 2, calculated by MELCOR code.